THE JOURNAL OF PHYSICAL CHEMISTRY C

Article

pubs.acs.org/JPCC

Four-Fold Increase in the Intrinsic Capacitance of Graphene through Functionalization and Lattice Disorder

Michael A. Pope and Ilhan A. Aksay*

Department of Chemical and Biological Engineering, Princeton University, Princeton, New Jersey 08544, United States

Supporting Information

ABSTRACT: Graphene has been heralded as a promising electrode material for high energy and power density electrochemical supercapacitors. This is in spite of recent work confirming the low double-layer capacitance (C_{DL}) of the graphene/electrolyte interface limited by graphene's low quantum capacitance (C_Q), an effect known for the basal plane of graphite for over four decades. Consistent with this limit, much of the supercapacitor research implies the use of pristine graphene but, in contrast, uses a functionalized and defective graphene formed through the reduction of graphene oxide, without clarifying why reduced graphene oxide is needed to achieve high capacitance. Herein, we show that an optimal level of functionalization and lattice disorder in reduced graphene oxide yields a 4-fold increase in C_{DL} over that of pristine graphene, suggesting graphene-based materials can indeed be tailored to engineer electrodes with significantly higher gravimetric capacitance limits exceeding 450 F/g than what has been achieved (~ 274 F/g) thus far, even in nonaqueous electrolytes capable of high voltage operation.

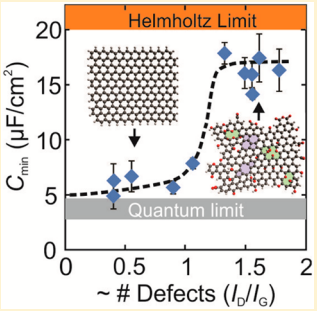

INTRODUCTION

Electrochemical supercapacitors are rechargeable energy storage devices capable of operating efficiently at a significantly higher power density and longer cycle life compared to current state-of-the-art battery technologies.[1] While these attributes have led to a myriad of applications, their low energy density (E < 10−20 Wh/kg) compared to Li ion technologies (150−200 Wh/kg) currently limits their widespread use,[2,3] inspiring a significant research effort to identify new materials and mechanisms which may be exploited to further boost the performance of this promising technology.

Capacitive charging arises by two possible mechanisms. In the first mechanism, when a potential is applied, the ions in the electrolyte adjacent to a charged conductor, typically a high specific surface area (SSA) carbonaceous material, rearrange to screen the resulting electric field.[1] A capacitor is formed across the subnanometer dielectric layer separating the electronic and ionic charge. The total capacitance of this interface is called the double-layer capacitance (C_{DL}). In this double-layer mechanism, charge does not cross the interface. The second mechanism involves a faradaic event where charge is partially or fully transferred from the electrolyte to the electrode through either specific adsorption or chemical reaction.[1] The additional capacitance that arises from these effects is typically referred to as pseudocapacitance (C_ϕ).

While C_ϕ can lead to enhanced charging, this mechanism is typically only observed in aqueous-based supercapacitors which exhibit a limited operating voltage (U) dictated by the electrochemical breakdown of water at $U \sim 1.2$ V.[1] On the other hand, most commercial supercapacitors employ aprotic, nonaqueous electrolytes capable of achieving 2.7−4 V operation, leading to higher E as $E \propto CU^2$.[3] Nonaqueous electrolytes typically reduce or eliminate contributions from C_ϕ by preventing the proton transfer reactions required for the redox behavior.[1] Typically, this leads to lower C_{INT} as only the double-layer mechanism is active. Thus, uncovering mechanisms that boost C_{INT} in such nonaqueous electrolytes will have a significant impact on the development of next generation supercapacitors.

Due to its potentially high SSA for capacitive charging, graphene has been touted as one of the most promising materials for next-generation supercapacitors.[4,5] However, C_{INT} of the pristine graphene/electrolyte interface is known to be low.[6] Further, excluding the edges, pristine graphene, by definition, contains no redox active functional groups and thus $C_{INT} \sim C_{DL}$ in a nonadsorbing electrolyte. At the high ionic strengths used in typical supercapacitors, the Debye screening length within the electrolyte approaches zero[7,8] and the C_{DL} of the graphene/electrolyte interface can be described in terms of two capacitances in series:

$$\frac{1}{C_{DL}} = \frac{1}{C_H} + \frac{1}{C_Q} \quad (1)$$

where the quantum capacitance, C_Q, describes the electronic contribution from the solid which is proportional to the square root of the electronic density of states (DOS) of graphene,[9,10] and C_H is the capacitance of the layer of ions in direct contact with the electrode,[11] called the Helmholtz (or Stern) layer. As capacitances in series add inversely, C_{DL} is limited by the smaller of C_H and C_Q. For pristine graphene, C_Q has been measured to be ~ 3−4 μF/cm²,[6] while C_H ranges from ~ 16 to

Received: August 3, 2015
Published: August 6, 2015

DOI: 10.1021/acs.jpcc.5b07521
J. Phys. Chem. C 2015, 119, 20369−20378

25 $\mu F/cm^2$ for typical electrolytes[1,11] and thus leads to the graphene/electrolyte interface exhibiting $C_{DL} \sim C_Q$. These observations were made when one side of a graphene sheet was exposed to the electrolyte during charging of the double layer.[6,12] However, as a porous supercapacitor electrode, graphene will be exposed to the electrolyte on both sides and must share the available DOS, N_0, between each of the electrode/electrolyte interfaces formed. According to Gerischer, $C_Q = \varepsilon\varepsilon_0\sqrt{N_0}$, where ε is the dielectric constant and ε_0 is the permittivity of free space; thus it is expected that C_Q, in this situation, would be reduced by a factor of $\sqrt{2}$. The decrease in C_{DL} resulting from such an effect was first proposed by Hahn et al.[13] to explain the reduction in C_{DL} observed when the pore walls of high SSA activated carbons approach the length scale of one graphene sheet in thickness. More recently, experiments by Stoller et al.[14] have provided support for this proposed effect by carrying out double-layer-capacitance measurements on large area graphene sheets deposited by chemical vapor deposition. Their electrochemical cell allowed the electrolyte to contact one or two sides of the sheet, and they found that C_{DL} was lower when two sides were exposed.

On the other hand, the interface formed between the electrolyte and other carbonaceous materials such as glassy carbon (GC) or the edge plane of highly oriented pyrolytic graphite (HOPG) exhibits much higher C_{INT}.[15] In aqueous electrolytes, $C_{INT} \sim 50-70$ $\mu F/cm^2$ has been observed and attributed to the high density of functional groups and dangling bonds present on these surfaces which contribute to C_ϕ.[15] While only a few studies have been carried out on these surfaces in nonaqueous electrolytes, it is generally accepted that the presence of functionalized edge-type sites leads to significantly enhanced C_{INT} compared to that of the basal plane of graphite. For example, polished GC is known to exhibit $C_{INT} \sim 20$ $\mu F/cm^2$ in various nonaqueous electrolytes as the high concentration of dopants present on the surface of this material causes C_{DL} to be limited by C_H rather than C_Q, implying that $C_Q \gg C_H$.[16,17] Recent theoretical work has demonstrated that defects and functional groups can significantly increase graphene's DOS, and simulations of double-layer capacitance suggest that this can lead to significant enhancement.[18,19]

This doping effect or the ratio of edge-plane to basal-plane sites on a high surface area carbonaceous electrode is often used to explain changes in a material's estimated C_{INT}.[20] However, such studies are typically carried out on porous electrodes where the true capacitance and ion-accessible surface area cannot be accurately determined due to complications arising from porosity related effects (see example in Figure S1).[20,21] Furthermore, if graphene is limited by C_Q, the measured C_{INT} is expected to be a function of the number of graphene sheets exposed to the electrolyte on both sides which is directly affected by aggregation and restacking of graphene during electrode fabrication. Contrary to complex porous systems, the two-dimensional (2D) nature of graphene and reduced graphene oxide, i.e., functionalized graphene sheets (FGSs), enables us to decouple these effects by studying well-defined, monolayer (ML) electrodes as model systems.[21] Previously, we demonstrated that such a system was capable of measuring C_{INT} of the graphene−electrolyte interface by depositing densely tiled MLs on either HOPG or Au passivated with alkanethiols. These two systems gave identical results which proved that ions did not penetrate between graphene and the substrate, allowing us to probe the capacitance of FGSs exposed to the electrolyte on one side only.

While FGSs share many similarities to pristine graphene, such as high SSA and 2D morphology, and can exhibit high electrical conductivity,[22] their honeycomb lattice is disrupted by functional groups and lattice defects,[23,24] the concentration of which depends on the specific reduction treatment. It is currently unknown how these defects in the graphene lattice might affect C_{INT}, specifically in commonly used nonaqueous electrolytes capable of high voltage operation. Thus, in this work, using the previously described model ML system,[21] we explore a large range of reduction conditions to determine how structural and chemical variations affect C_{INT} in the commonly used acetonitrile/tetraethylammonium tetrafluoroborate (AN/$TEABF_4$) electrolyte system. While attempts to dope pristine graphene with nitrogen, boron, or other dopants have only succeeded in changing C_{DL} by $\sim 1-2$ $\mu F/cm^2$,[12,25,26] we show that FGSs are intrinsically doped exhibiting 4-fold higher C_{DL} than what has been observed for pristine graphene.

EXPERIMENTAL METHODS

Exfoliation and Reduction of Graphite Oxide. Graphite oxide (GO) was donated by Vorbeck Materials Corp. This GO had a C/O ∼ 2.2 and no discernible graphite peak was observed by X-ray diffraction (XRD), indicating that this GO was well-oxidized.[24,27] Fused silica tubes were loaded with ∼ 75 mg of this powder and dried overnight under a stream of flowing dry nitrogen. The tubes were then evacuated and backfilled with ultrahigh purity (99.9995%) argon three times to replace any oxygen from the atmosphere which could potentially oxidize the FGSs at high temperatures after rapid thermal decomposition. The tubes were held under vacuum (∼ 10 Torr) while the GO loaded tube was passed into the hot zone of a Lindberg/Blue M tube furnace set at various temperatures ranging from 300 to 1100 °C for ∼ 60 s. The tubes were removed from the furnace and allowed to cool, and the powder was collected for subsequent analysis or thermal post-treatment.

The same GO was also used to prepare FGSs by hydrazine reduction according to the procedure outlined by Li et al.[28] A 10 mL suspension of 0.25 mg/mL graphene oxide in water was prepared by tip ultrasonicating (Vibracell, Sonics & Materials Inc., CT) GO at 40% amplitude for 15 min in ammoniated water with pH adjusted to 10. To this suspension, 10 μL of hydrazine hydrate was added and the resulting dispersion was heated by placing the vial in an oil bath set to 95 °C for 1 h. Unreacted hydrazine was removed by dialysis using 50 kDa dialysis tubing against 3 × 4 L of pH ∼ 10 ammoniated water in order to maintain effective charge stabilization.

Thermal Post-Treatments. Annealing of FGSs prepared by thermal exfoliation at 1100 °C for 60 s (as detailed above) was carried out at temperatures ranging from 1100 to 2100 °C in a resistively heated graphite furnace (Astro-1000, Thermal Technologies). The atmosphere was exchanged using three vacuum/purge cycles with ultrahigh purity (99.9995%) Ar. Under flowing Ar, samples were ramped to temperature at a rate of 5 °C/min and held for 2 h and then allowed to furnace cool. The furnace temperature was estimated by calibrating the furnace power with an optical pyrometer prior to the experimental series.

FGS Characterization. The C/O of FGSs was estimated by combustion analysis (Atlantic Microlabs, GA) and by energy dispersive X-ray spectroscopy (EDS, INCA x-act, Oxford

DOI: 10.1021/acs.jpcc.5b07521
J. Phys. Chem. C 2015, 119, 20369−20378

Instruments, U.K., attached to a VEGA1 scanning electron microscope (SEM), Tescan USA). For EDS, dense, smooth pellets of FGSs were prepared by compression of ∼5 mg of material in a pellet pressing die. Elemental compositions were determined by averaging at least four regions at 10 kV acceleration voltage and under 500× magnification. For samples containing low oxygen concentrations, spectra were recorded until at least 2000 counts of oxygen were detected. This procedure was found to give more consistent results than combustion analysis, especially for FGSs with high C/O. Powder XRD was carried out on thermally exfoliated and annealed FGSs using a Miniflex II (Rigaku Americas, Cu K_α radiation) diffractometer. Raman spectroscopy (Kaiser Optics, λ = 532 nm) was also carried out on dense pellets prepared using the same pellet pressing procedure as for EDS. The spectra were fit using the Breit−Wigner−Fano (BFW) line shape for the G-peak and a Lorentzian fit for the D-peak. The BFW fit is described by eq 2:

$$I = I_P \frac{(1 + (x - x_P)/q\gamma)^2}{1 + (x - x_P)^2/\gamma^2} = I_P\left(\frac{\gamma^2}{\gamma^2 + (x - x_P)^2}\right) \quad \text{as } q \to \infty \tag{2}$$

where x is the frequency, γ describes the peak width, I is the intensity, and q is a parameter used to quantify the asymmetry of the G-peak typically associated with Raman intensity at low frequencies (∼ 1100 and 1400 cm^{-1} associated with sp^3 hybridized carbons). The subscript "P" indicates the position (x_P) or intensity (I_P) of the peak.

Preparation of FGS ML Electrodes. Monolayers of FGSs were prepared by the method reported in our previous study.[21] A 5 mg sample of FGSs was dispersed in 20 mL of residue-free, electronic grade 1,2-dichloroethane (DCE) by ultrasonication at 40% amplitude and for 30 min, in an ice−water bath. Suspensions were then transferred to clean 15 mL glass tubes for centrifugation at ∼1500g (IEC Centra GP8R centrifuge, 218A rotor) for 60 min to remove any remaining FGS aggregates. Care was taken not to expose the suspension to any polymeric materials that dissolve in DCE (e.g., pipet tips, tube caps, syringe needles, etc.). Residues from these materials can build up at the air−water interface or adsorb on the FGSs. The concentrated supernatant was transferred to a glass syringe and dripped onto the clean air−water interface of a Langmuir−Blodgett (LB) trough (Nima Technology, maximum area of 280 cm^2) via Teflon tubing with interconnects made of solvent resistant poly(ether ether ketone). The LB trough was cleaned prior to deposition with electronic grade chloroform and filled three times with deionized water (18 MΩ resistance). On the third fill, the barriers were compressed and the air−water interface was cleaned by suction until the surface tension was measured to be that of pure water (∼ 72 mN/m) and did not change upon barrier compression or expansion, which is indicative of a clean air−water interface. A porous paper plate attached to a tensiometer was used to measure the surface pressure in the trough. The suspension was dripped onto the air−water interface at a rate of 0.1 mL/min. Typically 3−4 mL of this suspension was added to create a faint dark film of floating FGSs. Immediately after deposition, the barriers were compressed at a rate of 30 cm^2/min until the surface pressure was 25−30 mN/m.

Hydrazine reduced FGSs were deposited in a similar way. However, these FGSs were suspended in ammoniated water, which is not miscible with DCE. Therefore, we diluted the aqueous dispersion with methanol, a good water miscible spreading solvent,[29] at a volume ratio of 1:5 ammoniated water to methanol. Thermally exfoliated FGSs could also be deposited from water/methanol and water/ethanol suspensions. Such films yielded similar results to MLs deposited from DCE. However, FGSs with a high C/O were not as stable in pH adjusted aqueous dispersions and thus DCE was used instead.

Freshly cleaved HOPG blocks (SP-2 grade, Structure Probe Inc.) and flame-annealed Au-coated silicon wafers, prepared by e-beam evaporation (Angstrom Engineering) consisting of a 10 nm adhesion layer of Ti, followed by a 50 nm Pt diffusion barrier and a final 300 nm Au coating, were used as electrode substrates to be coated with the FGS MLs. These were placed on clean glass slides in the trough subphase on the opposite side of one of the barriers (after compression) to the film. The electrodes were slid under the trough barrier and positioned under the LB film. Water was withdrawn from the subphase with a syringe pump until the ML of floating FGSs was lowered onto the electrodes. Coated electrodes were then removed from the trough and placed in an Ar filled glovebox on a hot plate set at 120 °C to dry overnight prior to electrochemical testing. Au substrates coated with FGS MLs were placed in 1 mM hexadecanethiol (HDT) solution for at least 4 h prior to electrochemical testing to block any exposed Au.

Characterization of Monolayer Electrodes. Electrochemical characterization was carried out in an electrode holder described previously.[21] Monolayer coated electrodes were spring loaded in the electrode holder against an O-ring in order to define the geometric surface area (A_G) of the electrode exposed to the electrolyte. However, the use of nonaqueous electrolytes required switching from Viton or silicone O-rings (as described previously[21]) to a perfluoroelastomer (Kalrez, McMaster-Carr) O-ring to minimize swelling. The cell was filled with 5 mL of 0.1 M tetraethylammonium tetrafluoroborate ($TEABF_4$) in acetonitrile (AN). A Pt quasi-reference electrode and a Pt wire counter electrode were used. The potential of the reference electrode was determined after testing each ML by measuring the redox potential of ferrocene dissolved in the supporting electrolyte. Each ML electrode was analyzed by cyclic voltammetry at 100 mV/s followed by electrochemical impedance spectroscopy (EIS) using a perturbation amplitude of 10 mV over a frequency range of 1 Hz−100 kHz using an SP-300 potentiostat (Bio-Logic USA). The dc potential was held for 2 min before each EIS measurement was started. The capacitance was estimated from EIS testing using eq 3:

$$C_{DL} = \frac{1}{2\pi f(-Z'')} \tag{3}$$

where f is the measurement frequency and Z'' is the imaginary component of the impedance. Samples were first tested in a voltage window of −0.5 to 0.5 V vs open circuit potential and then in an expanded window of −0.7 to 1 V, beyond which faradaic currents due to residual oxygen and water in the electrolyte were observed. Also, the potential window was kept small enough to avoid intercalation effects which have been observed in similarly prepared porous FGS films at potentials beyond ±1 V vs open circuit.[30] All EIS measurements were carried out by starting at the most negative potentials and stepping the dc potential more positive.

DOI: 10.1021/acs.jpcc.5b07521
J. Phys. Chem. C 2015, 119, 20369−20378

After electrochemical testing in the supporting electrolyte (0.1 M $TEABF_4$/AN), 100 μL of 5 mM ferrocene in AN was added to the cell and cyclic voltammetry was carried out over a series of scan rates from 10 to 2000 mV/s. As mentioned above, this was used to define the reference potential but was also used to estimate the geometric surface area (A_G) of each ML electrode. A_G was determined from the peak current using the known diffusivity of ferrocene ($D \sim 2.4 \times 10^{-5}$ cm^2 s^{-1}),[31] scan rate (ν), and the concentration of ferrocene (C^*) using eq 4, which is derived for a reversible one electron transfer reaction:[31,32]

$$i_p = 0.4463\left(\frac{F^3}{RT}\right)^{1/2} A_G D^{1/2} C^* \nu^{1/2} \quad (4)$$

where F is the Faraday constant, R is the gas constant, and T is the temperature. Typically this area was estimated to be between 0.35 and 0.4 cm^2, depending on the level of O-ring compression and its degree of swelling. A_G is not the true surface area but the projected area of the electrode since the electrode features (roughness) are much smaller than the length scale associated with diffusion of ferrocene to the electrode surface at the scan rates used to obtain the cyclic voltammograms (CVs).[31]

Since the capacitance depends on the true surface area (A_T) exposed to the electrolyte and not A_G, we used a combination of SEM and atomic force microscopy (AFM) to estimate A_T. The relative coverage (A_R) or projected surface area of FGSs on the surface was estimated by pixel counting (Matlab) based on the secondary electron contrast differences between the Au and FGS coating. The surface roughness ($S_R \equiv A_T/A_G$) of each ML coating was estimated using contact-mode AFM (MultiMode/Digital Nanoscope IIIa system, Veeco Instruments) using NP-S tips (radius of curvature < 10 nm). AFM images of at least four different 5 × 5 μm locations were used to estimate the average S_R.

The electrochemical behavior of the FGS MLs was also compared to GC electrodes (SPI-Glas 25 grade, 10 × 10 × 2 mm blocks, Structure Probe Inc.). GC blocks were polished to a mirror finish using a suspension of 0.05 μm aluminum monohydroxide and a felt polishing pad (Buehler). Electrodes were then rinsed with deionized water and blow dried. No electrochemical activation/pretreatment of the GC was carried out prior to electrochemical characterization.

Preparation and Characterization of Thick Film Electrodes. Electrodes were prepared by dispersing 100 mg of the FGSs in 200 mL of water using a small amount of sodium dodecyl sulfate (SDS, 0.45 mM) to facilitate wetting of the hydrophobic powder by the water. This mixture was horn ultrasonicated for 1 h. Afterward, 25 μL of a 60 wt % Teflon emulsion was added to the dispersion. The mixture was then flocculated by adding sodium chloride to the dispersion (0.2 M), vacuum filtered and rinsed with deionized water to remove residual SDS and sodium chloride. The filter cake was chopped up into a fine powder and pressed into an aluminum mesh to yield an electrode with an FGS mass loading of ~ 3.5 mg/cm^2. From these dry electrodes, supercapacitors were assembled in standard CR2032 coin cells (MTI Corp.) in an Ar-filled glovebox (less than 1 ppm O_2 and H_2O) using 1 M $TEABF_4$ in AN. The single electrode capacitance is reported from the two electrode measurements using eq 5:

$$C = 2\frac{i}{\nu m} \quad (5)$$

where m is the mass of FGS in one of the electrodes. The capacitance in μF/cm^2 was estimated by dividing C by the surface area estimated using N_2 adsorption measurements fit using the BET theory,[33] and the pore-size distribution was calculated from the desorption branch according to the method of Dollimore and Heal.[34] Both materials show hysteresis in the pressure regime corresponding to pores with average radius (r_p) between ~ 2 and 60 nm. These measurements indicate that there is no significant difference in porosity between the two materials and we are above the pore size for which changes in capacitance are expected to occur based on the results of Chmiola et al.[35,36]

RESULTS AND DISCUSSION

Monolayer Morphology and Effective Surface Area. As shown in Figure 1, the projected surface area and roughness

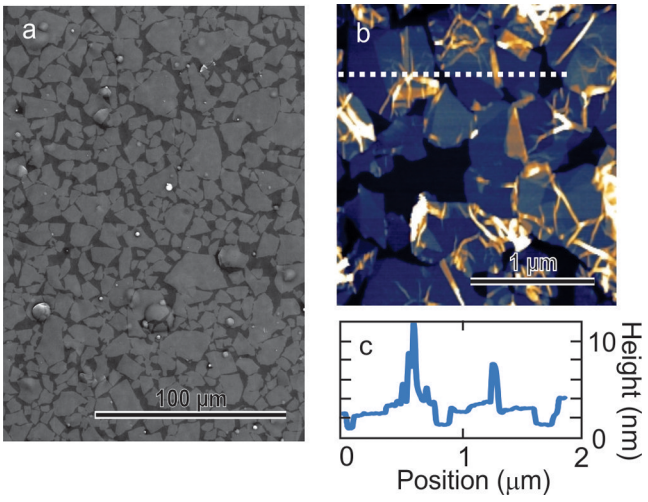

Figure 1. Morphology of FGS ML electrodes. (a) SEM image of graphene oxide ML (light contrast) on HOPG (dark contrast). (b) AFM image of FGS ML deposited on a mica substrate illustrating sheets ~ 1−2 nm thick and wrinkles with roughness of tens of nanometers. (c) Height profile, along the dotted line indicated by white dots in (b).

of the FGS MLs can be directly assessed by SEM and AFM and thus allow us to estimate C_{INT} independent of other parameters. The surface roughness ranged from 1.03 to 1.13 and tended to increase when MLs were prepared from FGSs that were annealed for 2 h at elevated temperatures (Figure 2a). This increase in surface roughness was a result of the FGSs transitioning from a relatively flat morphology to one with more wrinkles and folds as shown in Figure S2. The relative coverage of the various FGS MLs was found to vary between 80 and 90% (Figure 2b). The coverage tended to decrease with annealing temperature and time. Thus, while the 2 h annealed films were rougher, they were also less dense and thus corrections for surface coverage and roughness caused the actual ion-accessible surface area to differ by only 5−10% for all MLs analyzed.

To exclude the possibility that ions might access the space between the sheets and the substrates, we carried out measurements on both HOPG and FGS−Au−HDT substrates for which we obtained identical results despite large differences

DOI: 10.1021/acs.jpcc.5b07521
J. Phys. Chem. C 2015, 119, 20369−20378

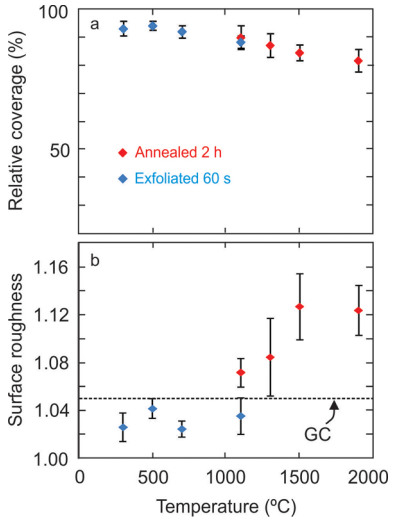

Figure 2. Estimating relative coverage and surface roughness of FGS ML electrodes. (a) Relative surface coverage determined by SEM and pixel counting in Matlab based on contrast differences between Au and FGS. (b) Surface roughness estimated by AFM for various FGS MLs. Dashed line corresponds to average surface roughness measured for GC. Error bars indicated standard deviation from at least 5 measurements.

between C_{INT} values of HOPG and Au, a result that was demonstrated in our previous work.[21] The only possible scenario potentially impacting our estimate of the ion-accessible surface area is that we cannot account for any internal porosity which might arise from wrinkled or folded sheets. While we expect this contribution to be negligible for samples with low surface roughness, as discussed above, the extent of wrinkling/folding became more extreme when samples were annealed above 1100 °C for 2 h, suggesting that the true surface area of these samples may be larger (i.e., may lower the estimated C_{INT}).

Electrochemical Analysis of Monolayers. The electrochemical cell shown in Figure 3a was used to estimate C_{INT} in 0.1 M $TEABF_4$ dissolved in AN for MLs prepared from several types of FGSs, determined by cyclic voltammetry and EIS, as a function of frequency and potential (E) as shown in Figure 3b,c. For comparison, the results for GC and HOPG are also shown and agree with previous studies.[9,17] In particular, the capacitance−potential (C−E) curve for HOPG demonstrates the well-known, U-shaped dependence (see inset in Figure 3c) of C_{DL} on the electrode potential with a capacitance minimum (C_{min}) between 3 and 4 $\mu F/cm^2$. For GC, the shape of the C−E curve is dictated by the charge, size, and orientation of the ions in the Helmholtz layer, all of which vary with potential.[1,11] C_{INT} of the FGS/electrolyte interface increased with annealing temperature approaching the GC response but then dropped significantly, approaching the response of HOPG, as the samples were annealed at higher temperatures. An intermediate case arose for FGSs annealed for 2 h at 1100 °C. In this case, C_{min} is drastically reduced when compared to the material exfoliated at 1100 °C but exhibited enhanced capacitance at high positive potentials. The CVs shown in Figure 3d indicate the same trends in capacitive charging current as measured by EIS.

To better understand the mechanisms responsible for the significant increases in C_{INT} of FGSs annealed at intermediate temperatures, we examine how the capacitance depends on frequency and applied potential. The CVs (Figure 3d) do not exhibit any peaks over a large potential range and thus indicate no obvious faradaic reactions that might contribute to C_ϕ. As shown in Figure 3b, HOPG, GC, and FGSs exhibit nearly identical frequency dependence over the range of potentials studied (see also Figure S3). There was only a slight increase in C_{DL} (10−20%) measured for each ML with increasing frequency over the range of 1−100 Hz. This relative increase was consistently observed for all samples (including various FGS MLs, HOPG, and GC) over all applied potentials and was likely due to some electrolyte leakage under the O-ring used to define the electrochemically active surface area. The upper frequency limit for measuring C_{DL} is defined by the RC time constant. Typically, the solution resistance in our cells was ∼100 Ω but varied depending on the exact position of the

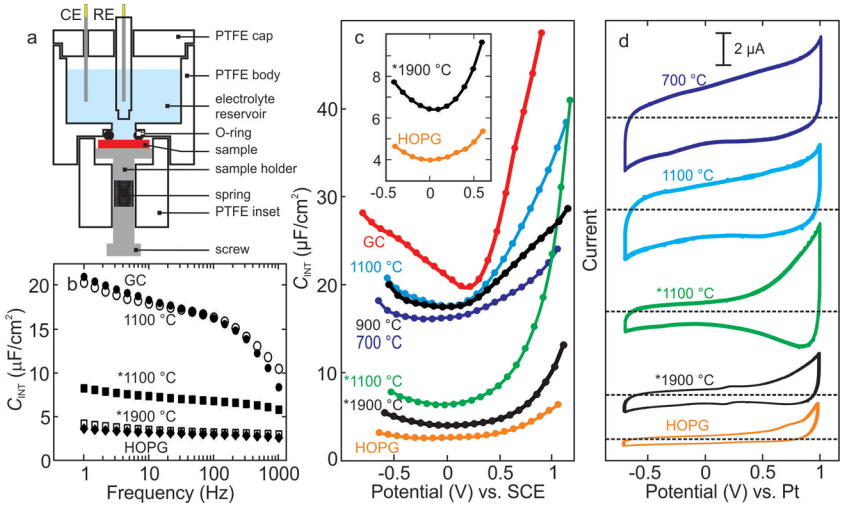

Figure 3. Electrochemical characterization of various FGS MLs. (a) Schematic of electrode holder. (b) C_{DL} measured by impedance spectroscopy as a function of measurement frequency at the open circuit voltage: GC (●); FGS (1100 °C, 60 s) (○); FGS (1100 °C, 2 h) (■); FGS (1900 °C, 2 h) (□); HOPG (◆). (c) C_{DL} measured at 100 Hz and at various potentials. Inset shows magnified view comparing the 1900 °C annealed sample with HOPG. (d) CVs of FGS MLs. Samples indicated with an asterisk were annealed for 2 h, while the other samples were exposed to the indicated furnace temperature for only 60 s. All electrochemical measurements were carried out in 0.1 M $TEABF_4$/AN.

DOI: 10.1021/acs.jpcc.5b07521
J. Phys. Chem. C 2015, 119, 20369−20378

reference electrode. Assuming a value of C_{DL}, an area of 0.35 cm^2, and a resistance of 100 Ω leads to a calculated characteristic frequency of $1/RC \approx 1-5$ kHz for the range of C_{DL} (5−20 $\mu F/cm^2$) measured which corresponded well to the upper limit for which we could measure the electrode's capacitance. Rearrangement of the ions in the Helmholtz layer and adsorption effects are also known to cause some frequency dispersion, especially in organic electrolytes which contain large, more polarizable anions/cations with weaker solvation shells compared to aqueous ones.[37−39] Since a slight upturn in the capacitance was observed at frequencies < 10 Hz, especially near the potentials for water oxidation and oxygen reduction, we report C_{INT} between 10 and 100 Hz. This procedure was suggested by Newman[40] as most faradaic reactions occur at slower rates.[41]

The shape of the CVs, the relatively constant capacitance with measurement frequency (independent of dc potential), and the fact that our measurements were carried out in an aprotic electrolyte all indicate that the electrodes can be approximated as ideally polarizable and any faradaic reaction contributions to capacitance measurements are negligible. These observations suggest changes in the C_{INT} are predominantly due to changes in C_{DL}.[1,15] Our measurements have also been confirmed in other nonaqueous electrolytes including propylene carbonate/$TEABF_4$ and several room temperature ionic liquids, suggesting that the observed enhancements to C_{DL} are applicable to a broad range of nonaqueous electrolyte systems.

For the sample annealed at 1100 °C for 2 h, the CV is not rectangular and we cannot definitively conclude that the increase is due to changes in C_{DL} alone. There are several possible explanations for this behavior. The effect may solely be due to C_{DL} if there was an asymmetric doping of the electronic density of states of holes rather than electrons within the material.[10] Alternatively this behavior could be described by potential-induced specific adsorption and desorption of anions.[1] This would contribute a faradaic pseudocapacitance to the measured capacitance at high positive potentials. This asymmetry was not observed in the smaller potential window, indicating that the 1100 °C FGS annealed for 2 h could also be considered ideally polarizable within the range of −0.5 to 0.5 V vs Pt but not necessarily in the extended voltage window of −0.7 to 1 V.

Chemical and Structural Evolution of FGSs with Heat Treatment. Clearly, the capacitance measured with FGS MLs changes significantly with annealing conditions. To understand how these various annealing conditions change the average structure and chemistry of the FGSs, we now discuss the results of elemental analysis and Raman spectroscopy. As shown in Figure 4a, C/O of the FGSs increases from ∼ 4 to 400 as the annealing temperature is increased or the samples are held in the furnace for longer times. Figure 4b shows the Raman spectra and peak fits for materials displaying two extremes of the D-band (∼1350 cm^{-1}) to G-band (∼1580 cm^{-1}) intensity ratio (I_D/I_G). The fits and fitted parameters for all annealing temperatures are given in Figures S4 and S5, respectively. As shown in Figure 4c, from 300 to 1100 °C, the I_D/I_G is nearly constant, reaching a shallow minimum near 700 °C and increasing as samples are exfoliated at higher temperatures. Thermal treatments at higher temperatures cause a significant drop in I_D/I_G. The I_D is proportional to the number of aromatic six-membered rings but is only active in the presence of defects (i.e., functional groups, vacancy or topological lattice defects)

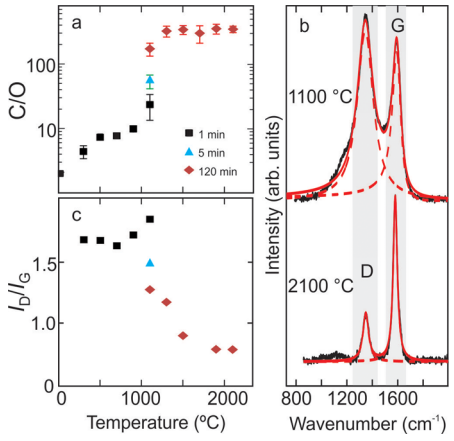

Figure 4. Estimating the degree of functionalization and defectiveness of FGSs. (a) C/O as a function of annealing temperature and time. Error bars indicate standard deviation between five different areas within a sample. (b) Raman spectra showing the characteristic D and G peaks for FGSs at two extremes of the I_D/I_G. Black lines show raw data; solid red lines show the fit obtained by deconvoluting the D and G peaks as shown by the dashed red lines. (c) I_D/I_G as a function of heat treatment.

around these aromatic regions, while the I_G is proportional to the number of any sp^2 carbon pair.[42] As the C/O increases (Figure 4a), we expect aromatic domains to grow, a claim supported by studies demonstrating the increase in electrical conductivity as a function of increasing temperature,[22] but at the same time, a fraction of the oxygen is removed from this material in the form of CO and CO_2 suggesting that lattice vacancies are also formed.[23,24] Therefore, the nonmonotonic changes in I_D/I_G below 1100 °C likely indicate the complex evolution of sp^2 carbon pairs, the growth of aromatic domains, and the evolution of lattice defects which maintain a high I_D/I_G as the C/O increases. As the samples are annealed at temperatures > 1500 °C, nearly all functional groups are removed and lattice defects are expected to anneal out,[43] leading to a significant drop in the I_D/I_G. At intermediate temperatures (∼ 1100 and 1300 °C), the vacancy and topological defects likely remain: In other carbonaceous materials it has been shown that such annealing only occurs at or above 1500 °C.[25] The decrease in I_D/I_G at 1100 °C with annealing time is correlated with a significant increase in C/O, suggesting that the drop in I_D/I_G is caused by the removal of defects in the form of residual functional groups. This explanation may also hold for the 1300 °C case. Changes in the Raman peak positions and widths shown in Figure S5 also support these conclusions which are further discussed in the Supporting Information.

Figure 5 shows the powder XRD profiles for the various FGSs. Samples annealed for only 60 s at temperatures below 1300 °C are largely amorphous, with the profiles exhibiting only broad reflections corresponding to d_{0002} for graphite ($2\theta \sim 27°$) and indicating an irregular spacing of the graphene sheets. However, since in the powder form it is impossible to prevent some regions from approaching regular spacing, the 300 °C annealed sample exhibits an additional peak near the angle corresponding to the graphite oxide spacing. This is due to the fact that fewer functional groups are removed as evidenced by the low C/O ∼ 4 which results after exfoliation and annealing at such low temperatures. The XRD profiles for the higher temperature, longer annealing time samples are shown in

DOI: 10.1021/acs.jpcc.5b07521
J. Phys. Chem. C 2015, 119, 20369−20378

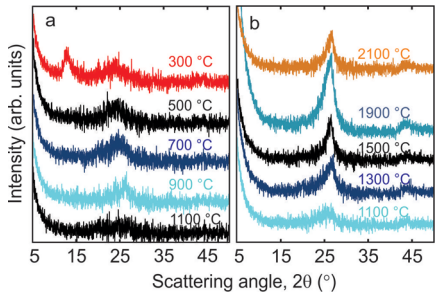

Figure 5. XRD profiles of FGS powders after exfoliation and annealing for (a) 60 s and (b) 2 h at the indicated temperatures.

Figure 5b. At annealing temperatures at and above 1300 °C, the graphitic peak ($2\theta \sim 27°$) becomes narrower, which indicates a higher degree of graphitic stacking order in the powders prior to dispersion. These results coincide with the observed changes in I_D/I_G which indicated an increase in the lateral crystallite size of pristine graphene domains within the FGSs over the same temperature range. The increased degree of graphitic stacking in these samples likely impeded our ability to disperse the FGSs as single sheets in the solvent used to disperse them at the air−water interface. The more wrinkled nature we observed for these samples could be a result of this restacking between adjacent sheets in the dry powder during the annealing process. Therefore, the XRD results suggest that the number of multilayer stacks in our MLs increased when samples were annealed at and above 1300 °C.

FGS Structure/Chemistry and Electrochemical Performance. To more clearly compare the capacitance with the structural and chemical changes which occur after the various thermal treatments, in Figure 6 we plot C_{min} against both the

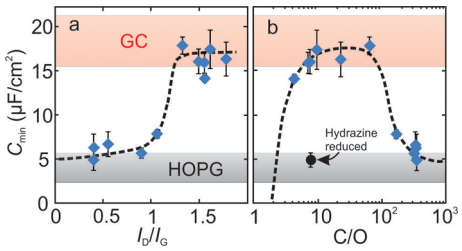

Figure 6. Capacitance as a function of material properties. C_{min} as a function of (a) integrated I_D/I_G and (b) C/O as measured by EIS at 10 Hz for samples evaluated from −0.5 to 0.5 V vs Pt. The pink and gray bars indicate the position of C_{min} ± 1 standard deviation for HOPG and GC, respectively. Points refer to FGSs which have been thermally reduced (◆) and hydrazine reduced (●). We previously demonstrated graphene oxide with a C/O ∼ 2, an electrical insulator, acts as a blocking layer which does not contribute to capacitance.[21] This is indicated by the expected diminishing of the capacitance as C/O → 2. All electrochemical measurements were carried out in 0.1 M $TEABF_4$ in AN.

I_D/I_G and C/O. Double-layer theory is only valid near the electrode's potential of zero charge[11] which, for carbonaceous electrodes in a nonadsorbing electrolyte, typically corresponds to the potential at C_{min} or the open circuit potential, which closely coincided in this work. C_{min} increased when samples were further annealed for 2 h at 1100 °C. The extended heat treatment significantly reduced the number of functional groups as indicated by the increase in C/O; however, as already discussed, at this temperature, significant annealing of lattice defects is not expected to occur.[43] To determine whether functional groups or lattice defects are required for the enhanced C_{DL}, we also tested FGSs produced by hydrazine reduction of graphene oxide.[44] This method leads to an intermediate C/O ∼ 8 and is thought to generate fewer lattice vacancies than the thermal reduction mechanism does.[45] The Raman spectrum of this material is shown in Figure S6. Hydrazine reduced FGSs were found to exhibit a low C_{min}. These results suggest that both a sufficiently high concentration of functional groups as well as lattice defects may be required to increase C_Q to such an extent that a 4-fold increase in C_{DL} is observed. These observations are supported by recent computational work that has predicted that topological defects such as Stone−Wales, divacancies, and di-interstitials in graphene can lead to a significant enhancement to the double-layer capacitance.[18]

As discussed in previous sections, there were minor changes in the morphology of FGSs, in particular, a more wrinkled morphology at annealing temperatures at or above 1300 °C leading to a larger surface roughness and the possible introduction of intersheet porosity which was not accounted for in our estimate of surface area. Accounting for this possible increase would tend to decrease our estimated C_{min} for these more wrinkled annealed materials resulting in an even larger drop in capacitance from the values measured for the low temperature annealed samples. Such a correction might also bring these results closer to the value measured for HOPG.

To complement our analysis with FGS MLs, we also carried out traditional capacitance measurements on thick film electrodes for which the surface area and porosity could be estimated by N_2 adsorption. In Figure 7a,b, we plot CVs and galvanostatic charge/discharge curves for samples which exhibited two extremes of C_{DL} estimated by our ML measurements (1100 °C, 60 s, and 1900 °C, 2 h annealed samples). When normalized by the N_2 accessible surface area, the capacitance estimated for relatively thick film (∼ 3.5 mg/cm^2) electrodes is similar to what was measured with the MLs, clearly demonstrating the significant difference in supercapacitor performance between the two materials. FGSs annealed at 1900 °C exhibited better rate performance (Figure 7b) which we attribute to the expected increase in electronic conductivity with annealing.[22] This highlights the expected trade-off between electrode conductivity and capacitance. The 1100 °C annealed sample displayed a capacitance of ∼ 20−25 μF/cm^2 at the various scan rates studied. This is slightly larger than our ML estimates (∼ 17 μF/cm^2 on average) which might be attributed to the slower measurement time scale of charge/discharge required for thick film electrodes due to a much higher resistivity compared to the ML case. At slower time scales it is possible to observe an additional pseudocapacitance contribution which acts in parallel to the C_{DL}. On the other hand, the 1900 °C annealed sample exhibited a much lower capacitance of 4−6 μF/cm^2 over the same range of scan rates which was similar to what we had measured with the ML system. To ensure that the lower C/O (corresponding to ∼ 3.8 atom % oxygen) and defective structure of FGSs annealed at 1100 °C did not negatively affect stability, we cycled these electrodes 10 000 times and observed less than 3% degradation in properties.

According to double-layer theory (eq 1), when C_Q is small (as is known to be the case for graphene[6,12]), the only way to observe such a significant change in C_{DL} is through an increase in C_Q. Using eq 1 and assuming $C_H \sim 20$ μF/cm^2, it is possible

DOI: 10.1021/acs.jpcc.5b07521
J. Phys. Chem. C 2015, 119, 20369−20378

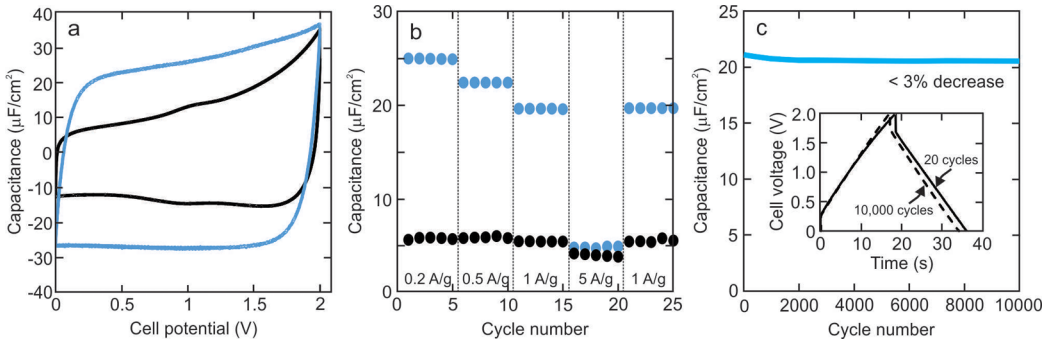

Figure 7. Performance of two-electrode cells fabricated from thick FGS electrodes. Data for supercapacitors fabricated using electrodes composed of FGSs annealed at 1100 °C for 60 s are shown in blue, and FGSs annealed at 1900 °C for 2 h are shown in black. (a) Capacitance estimated by cyclic voltammetry carried out at 20 mV/s. (b) Capacitance estimated by galvanostatic charge/discharge testing between 0 and 2 V at various current densities. (c) Capacitance estimated by galvanostatic charge/discharge testing between 0 and 2 V for FGSs annealed at 1100 °C for 60 s as a function of cycle number carried out at a current density of 1 A/g. Inset compares charge/discharge curves at 20th and 10000th cycles. All capacitances are reported as single-electrode capacitances but were measured in a symmetric two-electrode configuration using standard stainless steel coin cells (R2032) and an FGS loading of 3−4 mg/cm^2.

to estimate C_Q or, alternatively, the average DOS, N_0, using the relationship derived by Gerischer[10] for the various FGSs, as shown in Figure 8. Since C_{DL} measurements were carried out with one side of a FGS exposed to the electrolyte, the N_0 estimated is for the entire FGS as electronic states do not need to be shared in this case. However, to estimate the practical, theoretical limits of a graphene-based supercapacitor where all 2630 m^2/g of surface area is exposed requires that charging occur on both sides of the sheets. As illustrated in Figure 8, to simulate this scenario, we distribute the calculated N_0 between each side and recalculate C_Q and C_{DL}. This result allows us to predict the theoretical capacitance limit ($C_{G,theor.}$ in F/g) for electrodes based on the measured C_{DL} of our defective FGSs if all 2630 m^2/g of SSA were available to the electrolyte ($C_{G,theor.} \propto SSA\ C_{DL}$). As shown in Figure 8b, this estimate depends on the assumed C_H (i.e., the electrolyte used) and thus we show estimates for several values of C_H within the typical 16−25 μF/cm^2 range.[11] Using eq 1, $C_{DL} \sim C_Q$ when $C_Q \ll C_H$ leading to a low $C_{G,theor.}$, and as a result, $C_{G,theor.}$ is insensitive to variations in C_H clearly negating any explanations for our observed changes in terms of changes in C_H. On the other hand, $C_{G,\ theor.}$ for FGSs doped with functional groups and defects (i.e., high C_Q) approaches a much higher limit which depends on the electrolyte through C_H. The FGSs exhibiting the highest C_{DL} have the potential to achieve C_G approaching 450 F/g. Thus, electrodes with properties similar to pristine graphene, highly reduced or annealed FGSs, may reach a limit about one-fourth of this value due to the low C_Q. As shown by the dashed lines linking Figure 8, there is less than a 5% drop in $C_{G,theor.}$ between the cases where one side versus two sides of a sheet are exposed to the electrolyte. This is because there are ample states to distribute to each of the two double-layers formed on either side. On the other hand, the pristine graphene/electrolyte interface is significantly affected and decreases by 20−25% when a double-layer must be supported on both sides of a sheet. Therefore, the C_{DL} or $C_{G,theor.}$ of sufficiently functionalized and defective FGSs will be relatively insensitive to the number of restacked layers or the effective surface area of aggregated FGS electrodes in contrast to what is expected from a material with low C_Q.[13,14,46]

From our results, it is clear that the production method and annealing temperature used to make FGS electrodes significantly affects the C_{DL} of the FGS/electrolyte interface. Thus, in addition to changes in the SSA of electrodes used in electrochemical double layer capacitors (EDLCs), differences

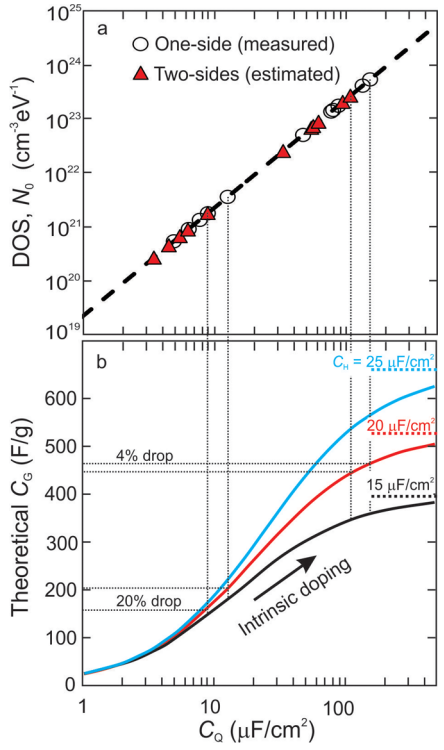

Figure 8. (a) Estimates of C_Q and N_0 calculated from the measured values of C_{DL} for the various FGS MLs tested. Since measurements were carried out on one side of a sheet, we first calculated C_Q according to eq 1, assuming C_H = 20 μF/cm^2. Gerischer's relationship, $C_Q = \varepsilon\varepsilon_0\sqrt{N_0}$, was used to estimate the total average DOS assuming the dielectric constant for graphite, ε = 3.28.[10,47] To estimate C_Q and N_0 for the case where both sides of the sheet are exposed to electrolyte, the previously calculated N_0 was divided by 2 and the same relationship was used to calculate the new C_Q. As illustrated by the dashed lines, these values are reduced by a factor of $\sqrt{2}$. (b) Illustration of the maximum theoretical C_G that can be achieved for various assumed values of C_H and over the range of C_Q estimated in (a). The dashed lines illustrate the expected insensitivity of the C_{DL} to electrolyte exposure on both sides of the sheet compared to a material which is limited by C_Q.

DOI: 10.1021/acs.jpcc.5b07521
J. Phys. Chem. C 2015, 119, 20369−20378

in thermal or chemical processing routes likely contribute to the wide range of C_{DL} values reported in the literature (e.g., 7−35 $\mu F/cm^2$ as estimated by reported C_G and SSA values).[4,5,48−51] The values of C_G reported in the literature for FGSs typically range from 100 to 200 F/g,[4,5,48−51] with several exceptional reports claiming ∼ 270 F/g.[52,53] These materials have not reached the theoretical limit because their ion-accessible SSA is low, implying that better techniques must be developed to enhance the ion-accessible SSA while, at the same time, using materials that exhibit high C_Q.

CONCLUSIONS

By measuring the interfacial capacitance of functionalized graphene monolayers in organic electrolyte, we determined how the double-layer capacitance of the graphene/electrolyte interface changes as a function of thermal and chemical treatments. A nearly 4-fold increase in double-layer capacitance was observed for materials containing a significant fraction of functional groups and lattice defects as inferred from elemental analysis and Raman spectroscopy. Functional groups or lattice defects alone were found insufficient to cause such an increase, suggesting that both are necessary. The observed changes were discussed in terms of increasing graphene's quantum capacitance through the incorporation of additional electronic states. While further increases in quantum capacitance may be possible through tailoring of graphene's structure, the maximum double-layer capacitance achieved in this study (∼ 17 $\mu F/cm^2$ near the potential of zero charge) suggests that graphene-based supercapacitors can exceed 450 F/g in high voltage nonaqueous electrolytes if the Helmholtz capacitance on the electrolyte side of the interface is at or above 20 $\mu F/cm^2$. Fabrication and testing of supercapacitors made from the same materials confirmed the relative trends in double-layer capacitance observed using the monolayer system and indicated that the defective and functionalized graphene exhibiting the highest C_{DL} did not impact stability as cycling 10 000 times caused less than 3% degradation.

ASSOCIATED CONTENT

Supporting Information

The Supporting Information is available free of charge on the ACS Publications website at DOI: 10.1021/acs.jpcc.5b07521.

Additional discussion on structural changes with annealing and additional AFM characterization of FGSs (PDF)

AUTHOR INFORMATION

Corresponding Author

*E-mail: iaksay@princeton.edu.

Present Address

M.A.P.: University of Waterloo, Waterloo, ON N2L 3G1, Canada.

Notes

The authors declare the following competing financial interest(s): The authors declare financial interest in Vorbeck Materials Corp. that manufactures functionalized graphene under the trade name Vor-x.

ACKNOWLEDGMENTS

This work was supported by an Army Research Office Multidisciplinary Research Initiative (W911NF-09-1-0476) and the Pacific Northwest National Laboratory (DE-AC05-76RL01830).

REFERENCES

(1) Conway, B. E. *Electrochemical Supercapacitors: Scientific Fundamentals and Technological Applications*; Kluwer Academic: New York, 1999.

(2) Gogotsi, Y.; Simon, P. True Performance Metrics in Electrochemical Energy Storage. *Science* **2011**, *334*, 917−918.

(3) Pope, M. A.; Korkut, S.; Punckt, C.; Aksay, I. A. Supercapacitor Electrodes Produced through Evaporative Consolidation of Graphene Oxide-Water-Ionic Liquid Gels. *J. Electrochem. Soc.* **2013**, *160*, A1653−A1660.

(4) Vivekchand, S. R. C.; Rout, C. S.; Subrahmanyam, K. S.; Govindaraj, A.; Rao, C. N. R. Graphene-based electrochemical supercapacitors. *Proc. - Indian Acad. Sci., Chem. Sci.* **2008**, *120*, 9−13.

(5) Zhu, Y.; Murali, S.; Stoller, M. D.; Ganesh, K. J.; Cai, W.; Ferreira, P. J.; Pirkle, A.; Wallace, R. M.; Cychosz, K. A.; Thommes, M.; Su, D.; Stach, E. A.; Ruoff, R. S. Carbon-Based Supercapacitors Produced by Activation of Graphene. *Science* **2011**, *332*, 1537−1541.

(6) Xia, J. L.; Chen, F.; Li, J. H.; Tao, N. J. Measurement of the Quantum Capacitance of Graphene. *Nat. Nanotechnol.* **2009**, *4*, 505−509.

(7) Chapman, D. L. A Contribution to the Theory of Electrocapillarity. *Philos. Mag.* **1913**, *25*, 475−481.

(8) Stern, O. The Theory of the Electrolytic Double Shift. *Z. Elektrochem. Angew. Phys. Chem.* **1924**, *30*, 508−516.

(9) Randin, J. P.; Yeager, E. Differential Capacitance Study on Basal Plane of Stress-Annealed Pyrolytic-Graphite. *J. Electroanal. Chem. Interfacial Electrochem.* **1972**, *36*, 257.

(10) Gerischer, H. An Interpretation of the Double Layer Capacity of Graphite Electrodes in Relation to the Density of States at the Fermi Level. *J. Phys. Chem.* **1985**, *89*, 4249−4251.

(11) Grahame, D. C. The Electrical Double Layer and the Theory of Electrocapillarity. *Chem. Rev.* **1947**, *41*, 441−501.

(12) Uesugi, E.; Goto, H.; Eguchi, R.; Fujiwara, A.; Kubozono, Y. Electric Double-Layer Capacitance Between an Ionic Liquid and Few-Layer Graphene. *Sci. Rep.* **2013**, *3*, 1−5.

(13) Hahn, M.; Baertschi, M.; Barbieri, O.; Sauter, J. C.; Kotz, R.; Gallay, R. Interfacial Capacitance and Electronic Conductance of Activated Carbon Double-Layer Electrodes. *Electrochem. Solid-State Lett.* **2004**, *7*, A33−A36.

(14) Stoller, M. D.; Magnuson, C. W.; Zhu, Y.; Murali, S.; Suk, J. W.; Piner, R.; Ruoff, R. S. Interfacial Capacitance of Single Layer Graphene. *Energy Environ. Sci.* **2011**, *4*, 4685−4689.

(15) Randin, J. P.; Yeager, E. Differential Capacitance Study on Edge Orientation of Pyrolytic-Graphite and Glassy Carbon Electrodes. *J. Electroanal. Chem. Interfacial Electrochem.* **1975**, *58*, 313−322.

(16) Kim, I.-T.; Egashira, M.; Yoshimoto, N.; Morita, M. Effects of Electrolytic Composition on the Electric Double-Layer Capacitance at Smooth-Surface Carbon Electrodes in Organic Media. *Electrochim. Acta* **2010**, *55*, 6632−6638.

(17) Lockett, V.; Sedev, R.; Ralston, J.; Horne, M.; Rodopoulos, T. Differential Capacitance of the Electrical Double Layer in Imidazolium-Based Ionic Liquids: Influence of Potential, Cation Size, and Temperature. *J. Phys. Chem. C* **2008**, *112*, 7486−7495.

(18) Pak, A. J.; Paek, E.; Hwang, G. S. Tailoring the Performance of Graphene-Based Supercapacitors Using Topological Defects: A Theoretical Assessment. *Carbon* **2014**, *68*, 734−741.

(19) Pak, A. J.; Paek, E.; Hwang, G. S. Impact of Graphene Edges on Enhancing the Performance of Electrochemical Double Layer Capacitors. *J. Phys. Chem. C* **2014**, *118*, 21770−21777.

(20) Pandolfo, A. G.; Hollenkamp, A. F. Carbon Properties and Their Role in Supercapacitors. *J. Power Sources* **2006**, *157*, 11−27.

(21) Pope, M. A.; Punckt, C.; Aksay, I. A. Intrinsic Capacitance and Redox Activity of Functionalized Graphene Sheets. *J. Phys. Chem. C* **2011**, *115*, 20326−20334.

(22) Punckt, C.; Muckel, F.; Wolff, S.; Aksay, I. A.; Chavarin, C. A.; Bacher, G.; Mertin, W. The Effect of Degree of Reduction on the

DOI: 10.1021/acs.jpcc.5b07521
J. Phys. Chem. C 2015, 119, 20369−20378

Electrical Properties of Functionalized Graphene Sheets. *Appl. Phys. Lett.* **2013**, *102*, 023114−023114−5.
(23) Schniepp, H. C.; Li, J. L.; McAllister, M. J.; Sai, H.; Herrera-Alonso, M.; Adamson, D. H.; Prud'homme, R. K.; Car, R.; Saville, D. A.; Aksay, I. A. Functionalized Single Graphene Sheets Derived from Splitting Graphite Oxide. *J. Phys. Chem. B* **2006**, *110*, 8535−8539.
(24) McAllister, M. J.; Li, J. L.; Adamson, D. H.; Schniepp, H. C.; Abdala, A. A.; Liu, J.; Herrera-Alonso, M.; Milius, D. L.; Car, R.; Prud'homme, R. K.; Aksay, I. A. Single Sheet Functionalized Graphene by Oxidation and Thermal Expansion of Graphite. *Chem. Mater.* **2007**, *19*, 4396−4404.
(25) Randin, J.-P.; Yeager, E. Effect of Boron Addition on the Differential Capacitance of Stress-Annealed Pyrolytic Graphite. *J. Electroanal. Chem. Interfacial Electrochem.* **1974**, *54*, 93−100.
(26) Zhang, L. L.; Zhao, X.; Ji, H. X.; Stoller, M. D.; Lai, L. F.; Murali, S.; Mcdonnell, S.; Cleveger, B.; Wallace, R. M.; Ruoff, R. S. Nitrogen Doping of Graphene and Its Effect on Quantum Capacitance, and a New Insight on the Enhanced Capacitance of N-Doped Carbon. *Energy Environ. Sci.* **2012**, *5*, 9618−9625.
(27) Hummers, W. S.; Offeman, R. E. Preparation of Graphitic Oxide. *J. Am. Chem. Soc.* **1958**, *80*, 1339−1339.
(28) Li, D.; Muller, M. B.; Gilje, S.; Kaner, R. B.; Wallace, G. G. Processable Aqueous Dispersions of Graphene Nanosheets. *Nat. Nanotechnol.* **2008**, *3*, 101−105.
(29) Kim, J.; Cote, L. J.; Kim, F.; Yuan, W.; Shull, K. R.; Huang, J. X. Graphene Oxide Sheets at Interfaces. *J. Am. Chem. Soc.* **2010**, *132*, 8180−8186.
(30) Hantel, M. M.; Kaspar, T.; Nesper, R.; Wokaun, A.; Kötz, R. Partially Reduced Graphite Oxide for Supercapacitor Electrodes: Effect of Graphene Layer Spacing and Huge Specific Capacitance. *Electrochem. Commun.* **2011**, *13*, 90−92.
(31) Bard, A. J.; Faulkner, L. R. *Electrochemical Methods: Fundamentals and Applications*, 2nd ed.; John Wiley & Sons, Inc.: New York, 2001.
(32) Nicholson, R. S.; Shain, I. Theory of Stationary Electrode Polarography. Single Scan and Cyclic Methods Applied to Reversible, Irreversible, and Kinetic Systems. *Anal. Chem.* **1964**, *36*, 706−723.
(33) Brunauer, S.; Emmett, P. H.; Teller, E. Adsorption of Gases in Multimolecular Layers. *J. Am. Chem. Soc.* **1938**, *60*, 309−319.
(34) Dollimore, D.; Heal, G. An Improved Method for the Calculation of Pore Size Distribution from Adsorption Data. *J. Appl. Chem.* **1964**, *14*, 109−114.
(35) Chmiola, J.; Yushin, G.; Gogotsi, Y.; Portet, C.; Simon, P.; Taberna, P. L. Anomalous Increase in Carbon Capacitance at Pore Sizes Less than 1 nm. *Science* **2006**, *313*, 1760−1763.
(36) Largeot, C.; Portet, C.; Chmiola, J.; Taberna, P.-L.; Gogotsi, Y.; Simon, P. Relation Between the Ion Size and Pore Size for an Electric Double-Layer Capacitor. *J. Am. Chem. Soc.* **2008**, *130*, 2730−2731.
(37) Kerner, Z.; Pajkossy, T. Impedance of Rough Capacitive Electrodes: the Role of Surface Disorder. *J. Electroanal. Chem.* **1998**, *448*, 139−142.
(38) Pajkossy, T. Impedance of Rough Capacitive Electrodes. *J. Electroanal. Chem.* **1994**, *364*, 111−125.
(39) Bozym, D. J.; Uralcan, B.; Limmer, D. T.; Pope, M. A.; Szamreta, N. J.; Debenedetti, P. G.; Aksay, I. A. Anomalous Capacitance Maximum of the Glassy Carbon−Ionic Liquid Interface through Dilution with Organic Solvents. *J. Phys. Chem. Lett.* **2015**, *6*, 2644−2648.
(40) Newman, J. Frequency Dispersion in Capacity Measurements at a Disk Electrode. *J. Electrochem. Soc.* **1970**, *117*, 198.
(41) Nisancioglu, K.; Newman, J. Separation of Double-Layer Charging and Faradaic Processes at Electrodes. *J. Electrochem. Soc.* **2012**, *159*, E59−E61.
(42) Ferrari, A. C.; Robertson, J. Interpretation of Raman Spectra of Disordered and Amorphous Carbon. *Phys. Rev. B: Condens. Matter Mater. Phys.* **2000**, *61*, 14095−14107.
(43) Campos-Delgado, J.; Kim, Y. A.; Hayashi, T.; Morelos-Gómez, A.; Hofmann, M.; Muramatsu, H.; Endo, M.; Terrones, H.; Shull, R. D.; Dresselhaus, M. S.; Terrones, M. Thermal Stability Studies of CVD-grown Graphene Nanoribbons: Defect Annealing and Loop Formation. *Chem. Phys. Lett.* **2009**, *469*, 177−182.
(44) Stankovich, S.; Dikin, D. A.; Piner, R. D.; Kohlhaas, K. A.; Kleinhammes, A.; Jia, Y.; Wu, Y.; Nguyen, S. T.; Ruoff, R. S. Synthesis of Graphene-based Nanosheets via Chemical Reduction of Exfoliated Graphite Oxide. *Carbon* **2007**, *45*, 1558−1565.
(45) Boehm, H. P.; Clauss, A.; Fischer, G.; Hofmann, U., Surface Properties of Extremely Thin Graphite Lamellae. In *Proceedings of the Fifth Conference on Carbon*; Pergamon Press: New York, 1962; pp 73−80.
(46) Wang, D.-W.; Li, F.; Wu, Z.-S.; Ren, W.; Cheng, H.-M. Electrochemical Interfacial Capacitance in Multilayer Graphene Sheets: Dependence on Number of Stacking Layers. *Electrochem. Commun.* **2009**, *11*, 1729−1732.
(47) Gerischer, H.; McIntyre, R.; Scherson, D.; Storck, W. Density of the Electronic States of Graphite: Derivation from Differential Capacitance Measurements. *J. Phys. Chem.* **1987**, *91*, 1930−1935.
(48) Stoller, M. D.; Park, S. J.; Zhu, Y. W.; An, J. H.; Ruoff, R. S. Graphene-Based Ultracapacitors. *Nano Lett.* **2008**, *8*, 3498−3502.
(49) Liu, W. W.; Yan, X. B.; Lang, J. W.; Xue, Q. J. Effects of Concentration and Temperature of EMIMBF4/acetonitrile Electrolyte on the Supercapacitive Behavior of Graphene Nanosheets. *J. Mater. Chem.* **2012**, *22*, 8853−8861.
(50) Liu, C.; Yu, Z.; Neff, D.; Zhamu, A.; Jang, B. Z. Graphene-Based Supercapacitor with an Ultrahigh Energy Density. *Nano Lett.* **2010**, *10*, 4863−4868.
(51) Lv, W.; Tang, D.-M.; He, Y.-B.; You, C.-H.; Shi, Z.-Q.; Chen, X.-C.; Chen, C.-M.; Hou, P.-X.; Liu, C.; Yang, Q.-H. Low-Temperature Exfoliated Graphenes: Vacuum-Promoted Exfoliation and Electrochemical Energy Storage. *ACS Nano* **2009**, *3*, 3730−3736.
(52) Yang, X.; Zhu, J.; Qiu, L.; Li, D. Bioinspired Effective Prevention of Restacking in Multilayered Graphene Films: Towards the Next Generation of High-Performance Supercapacitors. *Adv. Mater.* **2011**, *23*, 2833−2838.
(53) El-Kady, M. F.; Strong, V.; Dubin, S.; Kaner, R. B. Laser Scribing of High-Performance and Flexible Graphene-Based Electrochemical Capacitors. *Science* **2012**, *335*, 1326−1330.

DOI: 10.1021/acs.jpcc.5b07521
J. Phys. Chem. C 2015, 119, 20369−20378